Hydrodynamic Flow Focusing for Microfluidic Cell Sorting Chip

Ninad Dileep Mehendale[1] and Debjani Paul[1]

[1]Department of Biosciences and Bioengineering, Indian Institute of Technology Bombay, Mumbai, Maharashta, India400076

ninad.mehendale@iitb.ac.in , debjani.paul@iitb.ac.in

Abstract: Hydrodynamic flow focusing is an important requirement of microfluidic cell sorting devices. It allows the cells to arrive sequentially at the sorting location making detection easier. The simplest flow focusing configuration uses a three input Y-shaped microchannel. The sample enters the device from the central inlet and is squeezed by two side streams containing buffer (called "sheath" flows). The final focused width of the sample stream is purely a function of the flow-rates of central and sheath flows. In our simulations, the minimum width of 8 μm was observed when the ratio of the sheath flow to the sample flow was 5.5.The nature of the output barely changes even when the flow rates are increased or decreased, as long as all three flow rates are the same.

Keywords: Microfluidics, flow focusing, cell sorting, simulation, hydrodynamic focusing

1 Introduction

Flow focusing [1] technique is used to make cells arrive one by one at the sorting location. It is generally considered as the first stage of any passive cell sorting device [2]. Hydrodynamic flow focusing occurs when many flows are parallel to each other. The simplest configuration is the three-terminal Y-shaped device [3], which allows squeezing the flow from a small central inlet by two side streams (called "sheath" flows). The central flow is sandwiched between the two currents of sheath flows. The final focused width is purely a function of the flow-rates of central and sheath flows. Figure 1 shows the schematic diagram of two-dimensional flow-focusing.

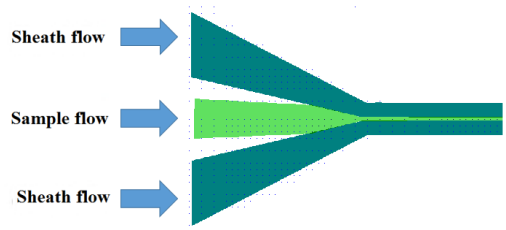

Figure 1: Schematic diagram of a simple flow-focusing device showing sample and sheath flows.

2 COMSOL simulation of flow-focusing

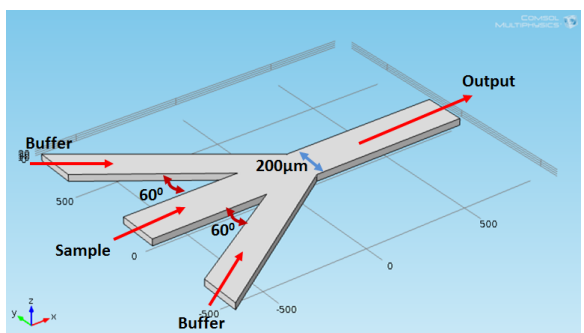

Figure 2: Flow focusing geometry
The figure shows the COMSOL model of the flow-focusing device. It has 200 μm wide channels and buffer inlets angled at 60^o with respect to the central sample input.

From literature [4] [5] [6] survey and taking into account our capabilities of microfabrication we decided that the channel width should be less than 500μm [7] but greater than 50μm. We

Excerpt from the Proceedings of the 2014 COMSOL Conference in Bangalore

chose 200μm [8] channel width for our flow focusing device (figure 2). Best flow-focusing in this device geometry is achieved when side (sheath) channels meet the central channel at 60 degrees. An angle of 30 degrees leads to very low pinching. On the other hand, an angle of 90 degrees leads to droplet generation (for two-phase flows) or a build-up of extreme pressures which may be detrimental for the cells. The channel height came out to be 30 μm using the negative photoresist SU-8 2025. SU-8 2025 is capable of generating feature heights between 25 and 50 μm.

The device geometry is simulated using COMSOL Multi-Physics software (version 4.3). We choose 3D simulation. Then we selected the microfluidics module. COMSOL software has all the essential physics such as, laminar flow, low Reynolds number etc. built in its microfluidic module. This is generally not available with other finite element simulators; hence COMSOL was used. Stationary study allows solving equations which do not vary with time. On the other hand, time-dependent study, as the name suggests, shows how the parameters vary with time. Time-dependent study generally takes much longer to simulate and also requires a huge amount of processing memory. As discussed later, in the current work we have reported both steady state and time dependent simulations. The Next step is generating the 3D model, which can easily be done by extruding the 2D geometry. The next step is to specify inlet and outlet velocities. We do so in terms of the flow rates. All three inlet flow rates were set as 10μl/min. We chose the boundary condition as "no-slip" condition. This boundary condition ensures that the fluid comes to rest at the channel walls. The next step is to create a mesh. We chose the "extremely fine" mesh option for better results. However, this kind of a mesh slows down the simulation. As shown in figure 4, the pressure is maximum at the inlets and then gradually decreases as we travel along the channel. A C-shaped pressure profile is observed at the junction of three channels. Figure 3 shows the magnitude of the velocities in five different cross-sections of the channel (YZ plane). From the figure, it appears that the velocity is maximum at the center of the channel.

Figure 5 shows a screen-shot of the COMSOL environment including the simulation results for flow-focusing. By varying the flow-rates different pinching widths were achieved. There is no theoretical limit to the pinching width as shown by **??**. When COMSOL simulations were carried out, we found a practical lower limit to the pinched flow. This is because back flow [9] hap-

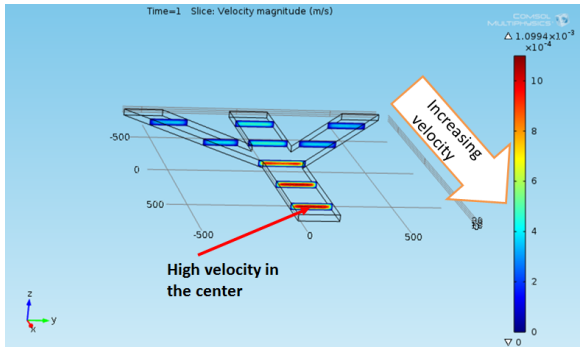

Figure 3: Velocity profile for flow-focusing device.
The flow velocity increases from zero value at the inlet to 1 mm/sec at the outlet. These simulation results show that once the cells enter the focused flow region, their velocity increases.

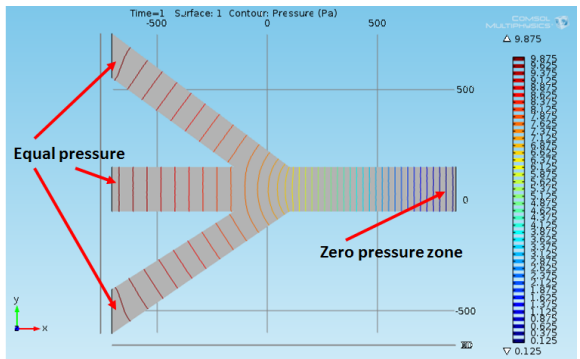

Figure 4: Pressure profile inside a flow-focusing device
It can be seen that pressure decreases from inlet (10 Pa) to outlet (0.1 Pa). A C-shaped pressure profile is seen to be created at the intersection of the channels.

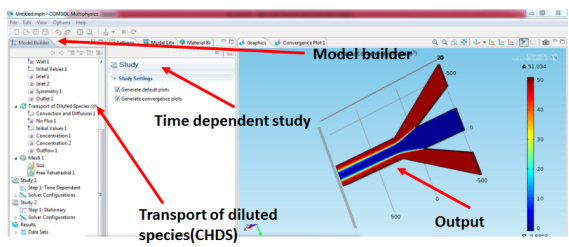

Figure 5: Screen-shot of the COMSOL environment after simulating the flow focusing device.
The figure shows the COMSOL simulation environment screen-shot. Both stationery and time-dependent studies were performed. To understand the time-dependent behavior, diluted species transport module was used to simulate flow-focusing.

Excerpt from the Proceedings of the 2014 COMSOL Conference in Bangalore

pens from the side channels into main channel. In our simulations, the minimum width was observed when the ratio of the sheath flow to the sample flow was 5.5.

3 Fabricating the flow focusing device

We designed the mask using AutoCAD. As shown in figure 6 , we set 1 unit = 1 micron. These masks are printed on standard A4 sized (210mm x 297mm) transparencies. Hence we first draw a rectangle of 210000 x 29700 units to indicate the transparency layer. Our wafer size is 2 inches, which is then indicated on the layer as a circular boundary (50800 unit diameter).This is because we use a MJB 3 (Karl Suss) mask aligner which can accommodate only 2 inch diameter wafers. Generally 12 such circles can fit on one A4 sized paper. Most of the microfluidic chips are bonded to glass cover slips for imaging. The glass cover slips that we use are generally 24

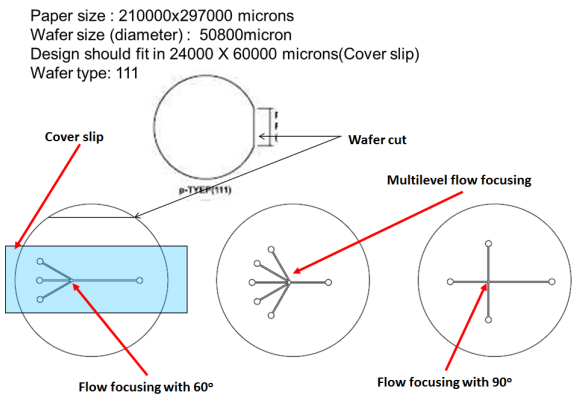

Figure 6: Parameters to consider during mask design.
The figure shows the design rules to be followed while designing a microfluidic chip. The mask should first fit on a 2 inch diameter wafer. The complete design must fit inside a glass cover slip of size 24 mm x 60 mm. The figure also shows three sample AutoCAD designs: the leftmost with flow focusing at 60 degrees, the central one with multiple focusing channels and the rightmost one for flow-focusing at 90 degrees.

mm x 60 mm. Hence our complete device must always fit inside 24000 units in any one direction and approximately in 50800 units in the other. Figure 6 shows different parameters to consider while designing the mask in AutoCAD. Generally we use a (111) wafer, which has a side cut for identification. The mask designer must also keep this aspect in mind during design.

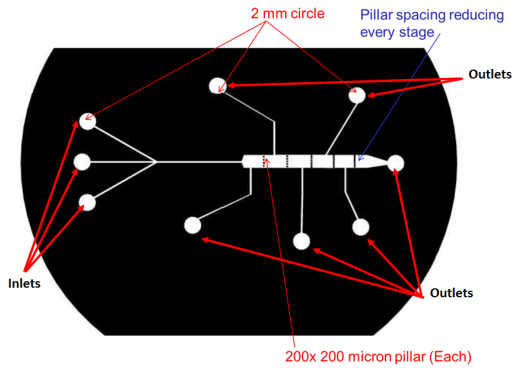

Figure 7: Autocad file layout file for design 1

Figure 7 shows the AutoCAD design file layout (in .dgn format) for a combined flow focusing and pillar-based cell sorting device (Design 1). There are 2mm wide circles to punch holes for inlets and outlets. All the channel widths were 200 μm and the main sorting channel was 1.2mm wide. The main channels consist of several lines of square pillars with decreasing pillar separation. Each pillar is 200 micron in size. Design 1 has five rows of pillars, with large gaps between the rows. Pillar spacing goes on reducing in each successive stage. After each stage, there is a separate output to collect the cells blocked at that particular stage.

The protocol for making the master is as follows:

- Heat wafer at 125 °C for 20 minutes to dehydrate.
- Spin coat SU-8 2025 resist with the following parameters:
  1. spreading spin: 500 rpm for 20 seconds.
  2. Increase speed from 500 rpm to 2500 rpm with a step of 204 rpm.
  3. Spinning at 2500 rpm for 45 seconds .
- Soft-bake at 65 °C for 3 minutes and ramp up to 95 °C. Hold at 95 °C for 5 minutes.
- UV exposure for 45 seconds (Karl Suss MJB3).
- Post-exposure baking at 65 °C for 1 minute. Ramp up to 95 °C and hold at 95 °C for 5 minutes.

Excerpt from the Proceedings of the 2014 COMSOL Conference in Bangalore

- SU-8 development with SU-8 developer in a petridish by gently swirling for 4 minutes.
- Wash off SU-8 developer from the master with IPA and dry with N2.

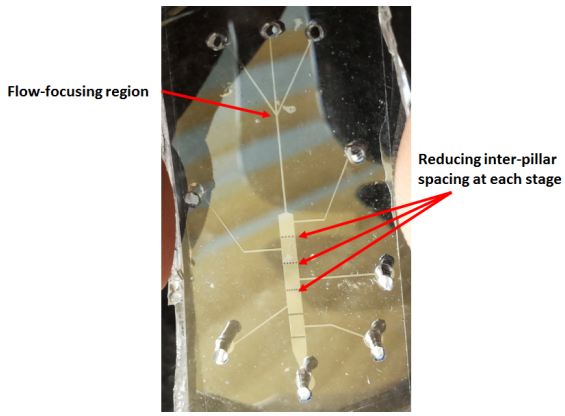

Figure 8: Final microfluidic device (flow focusing and cell sorting) after plasma bonding.

After master preparation PDMS (Polydimethylsiloxane) elastomer is used (mixing at 10:1 ratio of base to curing agent) to mold the device. Liquid PDMS after mixing is degassed in a desiccator to remove bubbles and then poured on the master. The PDMS-covered mold is transferred into an oven. After heating at 65 °C for 45 minutes, cured PDMS is removed from the master with the help of a sharp knife. Holes for inlet are made with a biopsy punch of 1.5 mm diameter. This PDMS chip is then bonded to a glass cover slip with oxygen plasma. The chip and the Piranha-cleaned glass cover slip are kept in plasma for 90 seconds. As shown in 8, the complete microfluidic chip is ready to use after bonding.

4 Results

4.1 Imaging flow focusing in our microfluidic device

The devices were imaged in an Olympus inverted microscope using a 10X objective. Flow through the device was controlled using two 111 syringe pumps (double syringe) from Cole Parmer. Time lapse images were captured at an interval of 1 sec and analysed using the open source image processing software ImageJ. We followed this procedure to measure the focused width in our devices. In this experimental setup fluorescein is used as the sample and water as buffer. This was done to enable better visualization of the focused sample. Flow-rates were set at 10 μl/min. 10ml syringes with microfluidic connectors and tygon tubings were used.

4.2 Analysis of experimental data

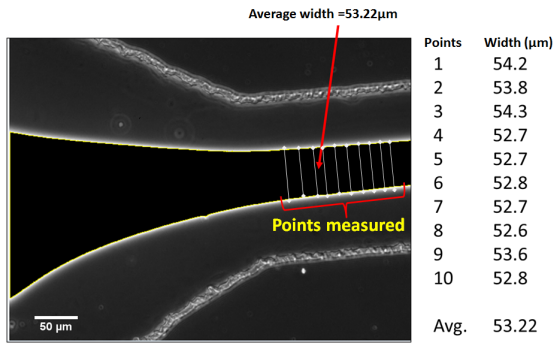

Figure 9: Measurement of the width of the squeezed channel
The figure shows how edge detection technique is used to determine the width of the sample liquid. When all the flow-rates are the same $\frac{1}{3}^{\text{rd}}$ of the channel width is occupied by the sample.

Figure 8 shows that the average width of the channel is about 53 μm which is approximately $\frac{1}{3}^{\text{rd}}$ of the total channel width. Once the image is captured in tif format it is processed via imageJ for edge detection. As seen in the figure, the complete region through which fluorescein was flowing was made black to achieve better contrast. For measurement of actual widths scale bar needs to be set in imageJ via a standard calibration image provided with the microscope. A set of 10 readings were taken manually (as shown in figure 8) and the average value with the standard deviation was reported.

4.3 Comparison between COMSOL results and experimental results

In figure 10, the COMSOL simulation output is shown on the left. The dark blue color is the buffer or the sheath liquid and the light blue color at the center is the squeezed sample. On the right is the actual image taken during experiments. The above image is obtained when all three flow-rates are kept the same. The nature of the output barely changes even when the flow

Excerpt from the Proceedings of the 2014 COMSOL Conference in Bangalore

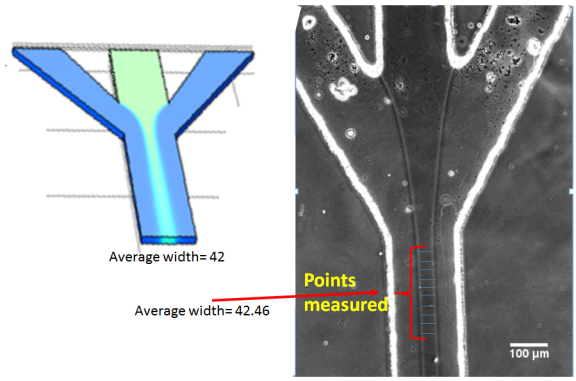

Figure 10: Comparison of COMSOL result with experiments under the same flow rates.
The figure on the left is the COMSOL simulation output. The dark blue colour indicates the buffer and the light blue colour at the center is the squeezed sample. The figure on the right shows the actual image taken during experiments performed with the same flow rates.

rates are increased or decreased, as long as all three flow rates are the same. This was tested experimentally over the flow range 1-1000μl/min

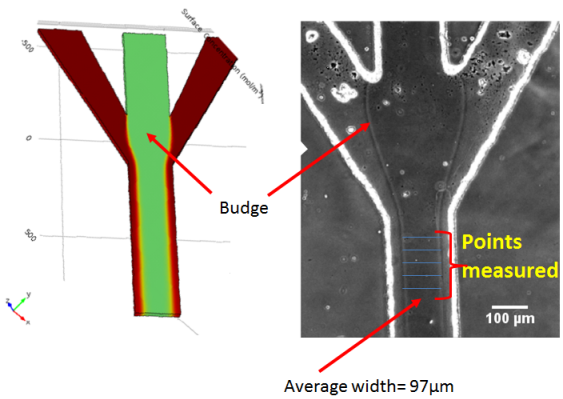

Figure 11: Comparison of COMSOL result with higher flow in the main channel
The figure on the left shows the COMSOL simulation output. The red fluid is the buffer and the light green fluid at the center is the squeezed sample. The figure on the right shows the actual image taken during experiments. At the junction, a bulge is seen as a result of the higher sample rate compared to the side channel buffers.

As seen in figure 11, when the sample flow-rate is increased compared to the sheath flow, a bulge is produced at the junction. It keeps on increasing till the bulge starts touching the walls. As soon as it touches the walls in the flow-focusing zone, back-flow starts.

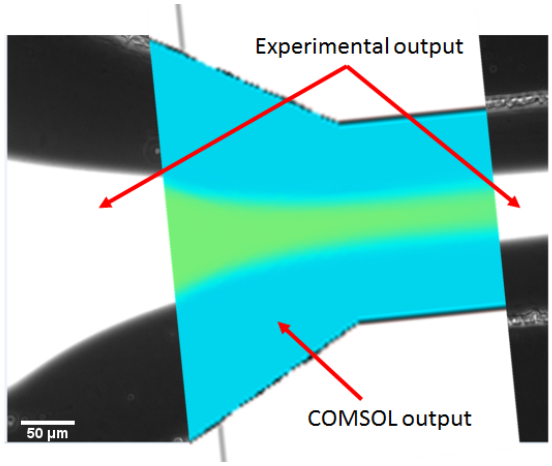

Figure 12: Overlapping of experimental and simulation results

Figure 12 is used to show that the simulation results match very well with what we get experimentally. The simulation output is cropped, rotated and its edges are matched with the experimental output figure. Figure 12 also shows that the matching is not exact. This could be resulting from device fabrication tolerances. From figures 10, 11 and 12, it is clear that the simulation and experimental results match very well.

4.4 Experiments with fluorescein

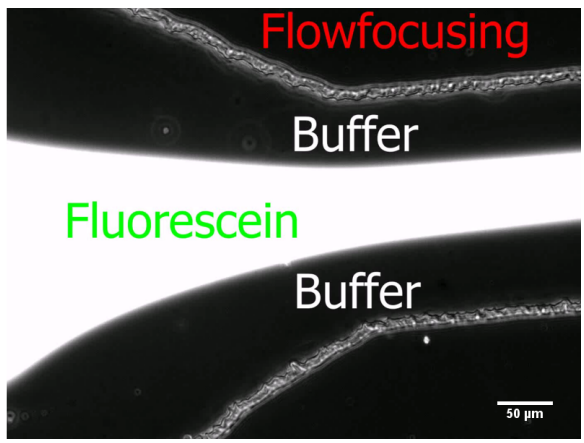

Figure 13: Flow-focusing achieved with fluorescein

Fluorescein gives good contrast during imaging in fluorescence mode and hence it was used to verify flow-focusing and effect of diffusion. As we can see in the figure 13 fluorescein was passed through the sample channel and the buffer liquid

Excerpt from the Proceedings of the 2014 COMSOL Conference in Bangalore

was DI water. The error in image processing is a lot less if we use fluorescein or fluorescently-tagged cells.

4.5 Minimum width achieved with Design 1

We have already seen that there exists an upper limit for sample flow-rate with respect to buffer flow-rate. In this section we will see that there also exists a lower limit for sample flow-rate with respect to buffer flow-rate. As seen in figure 14,

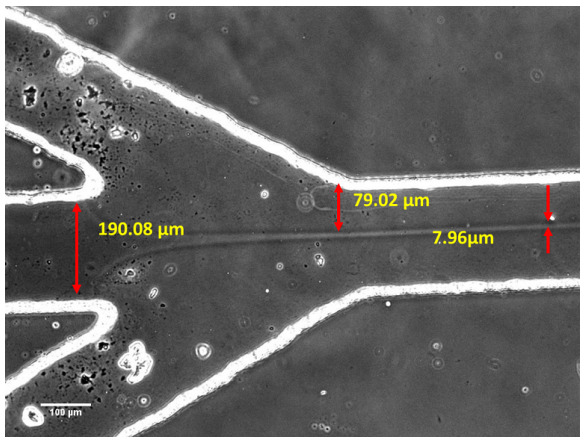

Figure 14: Minimum focusing width obtained with Design 1

an inlet sample width of 190 μm can be squeezed to around 8μm. This is achieved using a BD 1 ml syringe for the sample and a BD 10 ml syringe split into two by a T junction connector for the buffer. This was necessary as the flow focusing experiment was done using a single syringe pump. Here, the ratio of the sample fluid to the buffer fluid flow rate was around 1:5. All flow rates were set to 50μl/min. This can be achieved by selecting the option of 10 ml syringe in syringe pump. The same experiment was repeated with fluorescein and similar results were obtained again. Figure 15 confirms that the same minimum width of 8μm can be achieved for 200μm channels. Edge detection analysis was done using imageJ and the results were obtained by averaging 10 readings taken at random intervals in the focused region. If the sample flow rate is reduced further, the sample flow completely stops instead of achieving even smaller flow widths. In this case the buffer back flows into the sample channel. Similar results were also found via simulation. Hence, to achieve smaller focusing width we need to either reduce the channel dimensions or control the densities of the two liquids. But changing the two densities sometimes leads to droplet generation if fluids are bi-phasic.

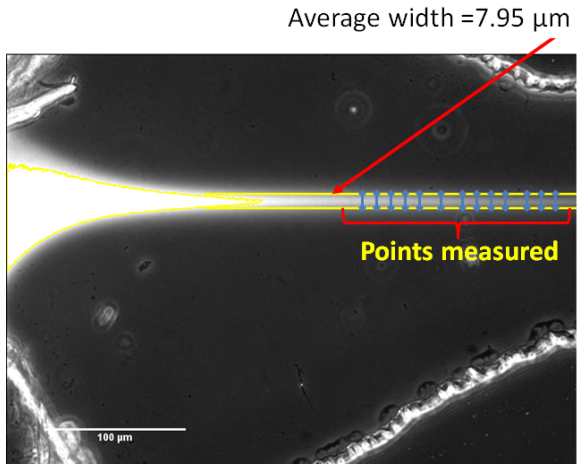

Figure 15: Estimation of minimum focusing width using fluorescein in sample channel

5 Conclusions

It is quite clear that the final focused width does not depend on the actual values of the flow rates, but depends on the ratio of sample flow (Q_2) to buffer flow (Q_1). The pinched width varies exponentially with the ratio of the two flow rates. This exponential curve has an upper limit and a lower limit, thereby limiting the minimum focus width. Ideally for cell sorting applications, the focus width should be comparable to the size of the cells to be sorted or even smaller. But we found that varying the ratio of the flow rates alone cannot achieve the desired width. Hence, dimensions of the channels should also be chosen depending up on the cell size. As shown in figure 16, the upper limit of $\frac{Q_1}{Q_2}$ is approximately 5. Above this value, the buffer starts flowing back into the sample channel. From the graph it is clear that the minimum width that can be achieved with our device is around 8μm. The graph shown in figure 16 is obtained by averaging 200 readings. The error bars indicate the standard deviations. To summarize, we have explored 2D flow-focusing. But the height of a microfluidic channel may not always be comparable to the size of a cell. When the channel height is much larger than the cell size, there is a possibility of two or more cells to be focused in two dimensions, but not in the 3rd dimension. In

Excerpt from the Proceedings of the 2014 COMSOL Conference in Bangalore

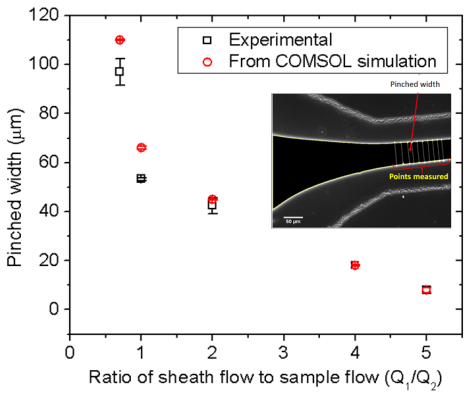

Figure 16: Focus width as a function of flow-rate ratio
Here y-axis depicts the focus-width in μm and x-axis depicts the ratio of sheath flow-rate to sample flow-rate $\frac{Q_1}{Q_2}$. The graph shows that the COMSOL simulation results are very close to the experimental data.

such cases we need to design a device for 3D flow focusing.

References

[1] S. L. Anna, N. Bontoux, and H. A. Stone, "Formation of dispersions using flow focusing in microchannels," Applied physics letters, vol. 82, p. 364, 2003.

[2] M. M. Wang, E. Tu, D. E. Raymond, J. M. Yang, H. Zhang, N. Hagen, B. Dees, E. M. Mercer, A. H. Forster, I. Kariv, et al., "Microfluidic sorting of mammalian cells by optical force switching," Nature biotechnology, vol. 23, no. 1, pp. 83–87, 2004.

[3] S.-W. Chung, J.-Y. Yu, and J. R. Heath, "Silicon nanowire devices," Applied Physics Letters, vol. 76, no. 15, pp. 2068–2070, 2000.

[4] P. Garstecki, I. Gitlin, W. DiLuzio, G. M. Whitesides, E. Kumacheva, and H. A. Stone, "Formation of monodisperse bubbles in a microfluidic flow-focusing device," Applied Physics Letters, vol. 85, no. 13, pp. 2649–2651, 2004.

[5] T. Ward, M. Faivre, M. Abkarian, and H. A. Stone, "Microfluidic flow focusing: Drop size and scaling in pressure versus flow-rate-driven pumping," Electrophoresis, vol. 26, no. 19, pp. 3716–3724, 2005.

[6] Q. Xu, M. Hashimoto, T. T. Dang, T. Hoare, D. S. Kohane, G. M. Whitesides, R. Langer, and D. G. Anderson, "Preparation of monodisperse biodegradable polymer microparticles using a microfluidic flow-focusing device for controlled drug delivery," Small, vol. 5, no. 13, pp. 1575–1581, 2009.

[7] Z. Nie, M. Seo, S. Xu, P. C. Lewis, M. Mok, E. Kumacheva, G. M. Whitesides, P. Garstecki, and H. A. Stone, "Emulsification in a microfluidic flow-focusing device: effect of the viscosities of the liquids," Microfluidics and Nanofluidics, vol. 5, no. 5, pp. 585–594, 2008.

[8] M. Kaya, S. Feingold, K. Hettiarachchi, A. P. Lee, and P. A. Dayton, "Acoustic responses of monodisperse lipid-encapsulated microbubble contrast agents produced by flow focusing," Bubble science engineering and technology, vol. 2, no. 2, p. 33, 2010.

[9] J. Rosell Lompart and A. M. GanCalvo, "Turbulence in pneumatic flow focusing and flow blurring regimes," Physical Review E, vol. 77, no. 3, p. 036321, 2008.

Excerpt from the Proceedings of the 2014 COMSOL Conference in Bangalore